Polyhedron 40 (2012) 134–144

Contents lists available at SciVerse ScienceDirect

Polyhedron

journal homepage: www.elsevier.com/locate/poly

Coordination polymeric materials in binary and ternary Cu(II)–tetracarboxylato–bipy systems: Structure–reactivity correlation in Cu(II)–(O,N) 1D–3D lattice assemblies

M. Menelaou [a,1], N. Lalioti [b], V. Psycharis [c], C.P. Raptopoulou [c], A. Terzis [c], C. Mateescu [d], A. Salifoglou [a,*]

[a] Department of Chemical Engineering, Aristotle University of Thessaloniki, Thessaloniki 54124, Greece
[b] Department of Chemistry, University of Patras, Patras 26500, Greece
[c] Institute of Materials Science, NCSR "Demokritos", Aghia Paraskevi, Attiki 15310, Greece
[d] Banat's University of Agricultural Sciences and Veterinary Medicine, Timisoara 300645, Romania

ARTICLE INFO

Article history:
Received 3 December 2011
Accepted 12 April 2012
Available online 21 April 2012

Keywords:
Copper
Tetracarboxylic acid
2,2′-Bipyridine
Structure–reactivity correlation
Coordination polymers

ABSTRACT

Cu(II) is a metal ion, the aqueous chemistry of which with carboxylic acids draws intense interest, targeting new materials and exemplifying diverse and unique structure–reactivity correlations. Driven by the need to explore the interplay of the chemical interactions of Cu(II) with polycarboxylic acid substrates and the association of such reactivity with lattice architecture and physicochemical properties, binary and ternary systems of Cu(II) with 1,2,3,4-cyclobutane-tetracarboxylic acid (H_4CBTC) and bipy (2,2′-bipyridine) were investigated. To this end, aqueous synthetic reactions of Cu(II) with H_4CBTC, under pH-specific conditions (pH 3), led to the isolation of the first species in the aforementioned binary system $[Cu_2(CBTC)(H_2O)_4)]_n{\cdot}2nH_2O$ (**1**). Aqueous synthetic chemical reactivity in the ternary Cu(II)–H_4CBTC–bipy system led to the isolation of the 1D polymer $[Cu(NO_3)_2(bipy)]_n$ (**2**). Complexes **1** and **2** were characterized by elemental analysis, spectroscopic techniques (EPR, FT-IR, UV–Vis and luminescence (**2**)), magnetic susceptibility, cyclic voltammetry (**2**) and thermogravimetric studies, and X-ray crystallography. The molecular lattice in **1** reveals the presence of Cu(II) units bound to (a) 1,2,3,4-cyclobutane-tetracarboxylate, and (b) water molecules, in a tetragonal pyramidal geometry, thereby projecting the unique chemical reactivity in the requisite system leading to a 3D lattice assembly. The presence of two types of channels in the solid state lattice of variable hydrophilicity/hydrophobicity signifies their unique nature in the coordination polymer and projects the importance of H_2O and its H-bonding ability in the assembly of **1**. The molecular lattice of **2** reveals the presence of Cu(II) ions bound to nitrate ions and 2,2′-bipy in an octahedral fashion, collectively leading to a 1D lattice assembly. The magnetic susceptibility and solid-state EPR data on **1** and **2** are consistent with the presence of Cu(II) in a tetragonal pyramidal and octahedral environment, respectively. Collectively, the physicochemical profiles of coordination polymers **1** and **2** earmark: (a) the influence of the polycarboxylic acid nature of the ligand on the chemical reactivity in binary and ternary systems, and (b) the critical nature of interactions in binary and ternary discrete Cu(II)–(O,N) species emerging in aqueous media and influencing the lattice assembly of Cu(II)–carboxylato materials of variable dimensionality (1D–3D), architecture and physicochemical properties.

1. Introduction

Copper has been recognized as an essential metal ion for all living organisms [1] and has been found in a variety of enzymes and proteins, such as blue copper proteins [2,3] and ceruloplasmin [4]. The absence of copper has been linked to pathophysiologically aberrant conditions, such as Menkes disease [5], while excess amounts of copper in tissues have been associated with Wilson's disease [6]. In abiotic systems, the interactions of divalent metal ions such as Cu(II) (and Co(II), Mn(II)) with various organic substrates of diverse chemical structure have been shown to afford novel materials with specific lattice architecture, magnetic and/or luminescence properties [7]. In all such cases, distinctly structured materials have arisen, all relying on well-designed binary and ternary interactions exemplified through unique reactivity pathways.

Through such chemical reactivity, copper emerges as a competent metal ion capable of coordinating organic substrates, bearing a

* Corresponding author. Tel.: +30 2310 996 179; fax: +30 2310 996 196.
E-mail address: salif@auth.gr (A. Salifoglou).
[1] Current address: Department de Química Inorgánica, Universitat de Barcelona, Diagonal 647, Barcelona 08028, Spain.

0277-5387/$ - see front matter © 2012 Elsevier Ltd. All rights reserved.
http://dx.doi.org/10.1016/j.poly.2012.04.012

distinct molecular signature and well-configured geometrical features, including α-hydroxycarboxylic acids, (poly)carboxylic acids and (carboxy)phosphonic acids. One such representative substrate is the low molecular mass 1,2,3,4-cyclobutane-tetracarboxylic acid (H_4CBTC), which is a multifunctional organic ligand containing key structural features (four carboxylate moieties) that render it capable of promoting metal ion binding. Concurrently, a well-known aromatic binder capable of promoting binary and ternary interactions with Cu(II) and third substrates is 2,2′-bipy. Based on the binding properties of 1,2,3,4-cyclobutane-tetracarboxylic acid and 2,2′-bipy mobilized toward Cu(II), solubilization essential to metallo-chemical interactions and conducive to the assembly of novel materials of variable dimensionality (1D, 2D or 3D coordination polymers) can be pursued [8,9].

Consequently, delineation of the role and influence of the metal ion and ligand nature on the lattice assembly, structure and properties of the arising species emerge as significant factors aiding in the understanding of the involved binary/ternary interactions and their link to the lattice properties of new materials with specific physicochemical properties. In this regard, investigation of the aqueous synthetic chemistry of Cu(II) with carboxylate binders, such as 1,2,3,4-cyclobutane-tetracarboxylic acid, and N,N-aromatic chelators, such as 2,2′-bipy, can shed light on the assembly of new inorganic–organic hybrids with well-defined physicochemical profiles. Prompted by that need, we report herein: (a) the pH-specific syntheses, isolation, spectroscopic and structural characterization, as well as magnetic and EPR studies of the first species arising from the binary/ternary Cu(II):1,2,3,4-cyclobutane-tetracarboxylic acid/2,2′-bipy system, and (b) the correlation of the observed chemical reactivity with the solid-state 1D–3D lattice assembly and architecture at the binary and ternary level.

2. Experimental

2.1. Materials and methods

All manipulations were carried out under aerobic conditions. $CuSO_4{\cdot}5H_2O$ was purchased from Mallinckrodt, $Cu(NO_3)_2{\cdot}2.5H_2O$ and 1,2,3,4-cyclobutane-tetracarboxylic acid (H_4CBTC) from Aldrich. KOH, NaOH, ammonia as well as 2,2′-bipyridine were supplied by Fluka. Nano-pure quality water was used in all reaction runs.

2.2. Physical measurements

FT-Infrared measurements were taken on a 1760X FT-Infra Red spectrometer from Perkin Elmer, using KBr pellets. UV–Vis measurements were carried out on a Hitachi U2001 spectrophotometer in the range 190–1000 nm. A ThermoFinnigan Flash EA 1112 CHNS elemental analyzer was used for the simultaneous determination of carbon, hydrogen and nitrogen (%). The analyzer operation is based on the dynamic flash combustion of the sample (at 1800 °C) followed by reduction, trapping, complete GC separation and detection of the products. The instrument is (a) fully-automated and controlled by PC via the Eager 300 dedicated software, and (b) capable of handling solid, liquid or gaseous substances. A major advantage of the instrument is that it can handle solid, liquid or gaseous substances.

A TA Instruments, model Q 600, system was used to run the simultaneous TGA–DTG experiments. The employed heating rate was 5 °C/min. The instrument mass precision is 0.1 μg. About 20 mg of sample was placed in an open alumina sample pan for each experiment. High purity air (80/20 in N_2/O_2) was used at a constant flow rate of 100 mL/min, depending on the conditions required for running the experiment(s). During the experiments, the sample weight loss and rate of weight loss were recorded continuously under dynamic conditions, as a function of time or temperature, in the range 30–700 °C. Prior to activating the heating routine program, the entire system was purged with the appropriate gas for 10 min, at a rate of 400 mL/min, to ensure that the desired environment had been established.

Emission and excitation spectra were recorded on a Hitachi F-700 fluorescence spectrophotometer from the Hitachi High-Technologies Corporation. The employed split widths (em, ex) were 5.0 nm, and the scan speed was 60 nm min^{-1}. All measurements were carried out at room temperature. The entire system was supported by the appropriate computer software, FL Solutions 2.1, running on Windows XP.

The EPR spectra of complexes **1** and **2** in the solid state were recorded on a Bruker ER 200D-SRC X-band spectrometer, equipped with an Oxford ESR 9 cryostat, operating at 9.61 GHz, 10 dB (2 mW) and at 4 K. Magnetic susceptibility data were collected on powdered samples of **1** and **2** with a Quantum Design SQUID susceptometer in the 2–300 K temperature range, under various applied magnetic fields. Magnetization measurements were carried out at three different temperatures in the field range 0–5 T.

Electrochemical measurements were carried out with a model PGSTAT30 potensiostat–galvanostat from Autolab Electrochemical Instruments. The entire system was under computer control and supported by the appropriate computer software, GPES, running on Windows XP. The employed electrochemical cell had platinum (disk) working and auxiliary (wire) electrodes. An Ag/AgCl electrode was used as the reference electrode. Thus, the derived potentials in the cyclic voltammetric measurements are referenced to that electrode. The water used in the electrochemical measurements was of nano-pure quality. KNO_3 was used as a supporting electrolyte. Normal solution concentrations used were 1–6 mM in electroanalyte and 0.1 M in supporting electrolyte. Purified argon was used to purge the solutions prior to the electrochemical measurements. Derived $E_{1/2}$ values are reported versus the Ag/AgCl electrode.

2.3. Synthesis of $[Cu_2(CBTC)(H_2O)_4)]_n{\cdot}2nH_2O$ (**1**)

$CuSO_4{\cdot}5H_2O$ (0.10 g, 0.40 mmol) and 1,2,3,4-cyclobutane-tetracarboxylic acid (H_4CBTC) (0.090 g, 0.40 mmol) were placed in a 50 mL round bottom flask and dissolved in 20 mL of water. The reaction mixture was then stirred at room temperature until both reactants were completely dissolved. The pH of the clear solution was adjusted to 3 with aqueous KOH (or NaOH, and/or ammonia). Subsequently, the reaction mixture was filtered and allowed to stand at room temperature. After a short period of time, blue cubic crystals grew out of solution by slow evaporation. The crystalline material was collected by filtration and dried in vacuo. Yield: 0.070 g (~76%). *Anal.* Calc. for **1** ($C_8H_{16}Cu_2O_{14}$ M_r 463.28): C, 20.72; H, 3.45. Found: C, 20.60; H, 3.43%.

2.4. Synthesis of $[Cu(NO_3)_2(bipy)]_n$ (**2**)

(a) $Cu(NO_3)_2{\cdot}2.5H_2O$ (0.40 g, 1.7 mmol) and 1,2,3,4-cyclobutane-tetracarboxylic acid (H_4CBTC) (0.20 g, 0.86 mmol) were placed in a 50 mL round bottom flask and dissolved in 20 mL of water. The reaction mixture was stirred at room temperature until both reactants were completely dissolved. Subsequently, 2,2′-bipy (0.13 g, 0.83 mmol) was dissolved in 5 mL of methanol and added to the reaction mixture dropwise. The reaction solution was then filtered and allowed to stand at room temperature. After a short period of time, blue crystals grew out of the solution by slow evaporation. The crystalline material was collected by filtration and dried in vacuo. Yield: 0.45 g (77.0%). *Anal.* Calc. for **2** ($C_{10}H_8CuN_4O_6$

M_r 343.74): C, 34.90; H, 2.32; N, 16.30. Found: C, 34.80; H, 2.22; N, 16.22%.

(b) A similar reaction was carried out in the absence of 1,2,3,4-cyclobutane-tetracarboxylic acid (H_4CBTC), affording morphologically identical blue crystals. $Cu(NO_3)_2{\cdot}2.5H_2O$ (0.40 g, 1.7 mmol) was placed in a 50 mL round bottom flask and dissolved in 10 mL of water. 2,2′-Bipy (0.53 g, 3.40 mmol) was dissolved in 5 mL of methanol and added to the reaction mixture dropwise. The reaction mixture was filtered and allowed to stand at room temperature. After a few days, a blue crystalline material was isolated. The FT-IR spectrum of the crystals and the X-ray unit cell determination of one of the isolated single crystals identified the material as compound **2**.

2.5. X-ray crystal structure determination

Single crystals of complexes **1** and **2** were obtained from aqueous solutions according to the described synthetic procedures. A single crystal with approximate dimensions 0.25 × 0.15 × 0.10 mm, for **1**, was taken from the mother liquor and immediately cooled to −100 °C. A single crystal with approximate dimensions 0.45 × 0.25 × 0.18 mm, for **2**, was mounted on a capillary. Diffraction measurements were run on a Rigaku R-AXIS SPIDER Image Plate diffractometer using graphite monochromated Cu Kα radiation. Data collection (ω-scans) and processing (cell refinement, data reduction and empirical absorption corrections) were performed using the CRYSTALCLEAR program package [10]. The structures of **1** and **2** were solved by direct methods using SHELXS-97 [11] and refined by full-matrix least-squares techniques on F^2 with SHELXL-97 [12]. A summary of the crystallographic data for **1** and **2** are given in Table 1.

Further experimental crystallographic details for **1**: $2\theta_{max}$ = 140°; reflections collected/unique, 7096/1344 [R_{int} = 0.0266]/1344; 109 parameters refined; $[\Delta/\sigma]_{max}$ = 0.001; $(\Delta\rho)_{max}/(\Delta\rho)_{min}$ = 0.376/−0.400 e Å^{-3}; R/R_w (for all data), 0.0268/0.0685 and GOF = 1.127. Further experimental crystallographic details for **2**: $2\theta_{max}$ = 128°; reflections collected/unique, 7631/1788 [R_{int} = 0.0248]/1788; 222 parameters refined; $[\Delta/\sigma]_{max}$ = 0.004; $(\Delta\rho)_{max}/(\Delta\rho)_{min}$ = 0.407/−0.287 e Å^{-3}; R/R_w (for all data), 0.0296/0.0763 and GOF = 1.086. All non-hydrogen atoms in **1** and **2** were refined anisotropically. All hydrogen atoms in **1** were located by difference maps but not refined. All hydrogen atoms in **2** were located by difference maps and refined isotropically.

Table 1
Summary of crystal, intensity collection and refinement data for $[Cu_2(C_8H_4O_8)(H_2O)_4]_n{\cdot}2nH_2O$ (**1**) and $[Cu(NO_3)_2(bipy)]_n$ (**2**).

	(**1**)	(**2**)
Formula	$C_8H_{16}Cu_2O_{14}$	$C_{10}H_8CuN_4O_6$
Formula weight	463.28	343.74
T (K)	173(2)	293(2)
λ (Å)	Cu Kα 1.54187	Cu Kα 1.54187
Space group	$I4_1/a$	$P\bar{1}$
a (Å)	24.7563(5)	7.4080(1)
b (Å)	24.7563(5)	9.8794(2)
c (Å)	4.7611(1)	10.0080(1)
α (°)	90.00	116.985(1)
β (°)	90.00	100.260(1)
γ (°)	90.00	103.275(1)
V (Å^3)	2917.96(9)	600.67(2)
Z	16	2
D_{calc} (mg m^{-3})	2.109	1.901
Absorption coefficient (μ) (mm^{-1})	4.366	2.960
Range of h, k, l	$-24 \leqslant h \leqslant 28$	$-6 \leqslant h \leqslant 7$
	$-20 \leqslant k \leqslant 29$	$-11 \leqslant k \leqslant 11$
	$-5 \leqslant l \leqslant 4$	$-11 \leqslant l \leqslant 11$
Goodness-of-fit on F^2	1.127	1.086
$R^{(1)}$	0.0253$^{(2)}$	0.0283$^{(2)}$
$R_w{}^{(1)}$	0.0677$^{(2)}$	0.0753$^{(2)}$

$^{(1)}R$ values are based on F values, R_w values are based on F^2. $R = \frac{\sum||F_o|-|F_c||}{\sum(|F_o|)}$, $R_w = \sqrt{\sum[w(F_o^2 - F_c^2)^2]/\sum[w(F_o^2)^2]}$.

$^{(2)}$[For 1272 (**1**) and 1703 (**2**) reflections with $I > 2\sigma(I)$].

3. Results

3.1. Syntheses

Compound **1** was synthesized through an expedient synthetic procedure, where Cu(II) sulfate and 1,2,3,4-cyclobutane-tetracarboxylic acid reacted in water with a molar ratio of 1:1 at pH 3 (Reaction (1)). The use of different inorganic bases (KOH, NaOH and ammonia) was crucial in the investigation of the binary system as they adjusted the pH of the reaction mixture to 3 with no evident participation, however, in the emerging lattice of the isolated compound **1**.

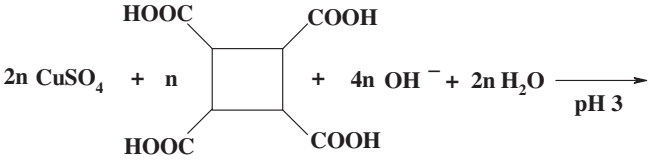

1,2,3,4-cyclobutane-tetracarboxylic acid (H_4CBTC)

$$[Cu_2(C_8H_4O_8)(H_2O)_4]_n \cdot 2n\,H_2O \quad + \quad 2n\,SO_4^{2-} \qquad \text{(Reaction1)}$$

Furthermore, in an effort to delve into the chemical reactivity of the aforementioned system, a third reagent, 2,2′-bipyridine, was employed, thereby turning the system into a ternary reaction mixture. All three reagents reacted in a mixture of CH_3OH/H_2O with a molar ratio of 2:1:1. However, the employment of the H_4CBTC binder did not result in its incorporation into the coordination sphere of Cu(II). On the contrary, a new inorganic–organic hybrid (compound **2**) emerged, in which Cu(II) ions are only coordinated by nitrate ions and 2,2′-bipyridine (Reaction (2)).

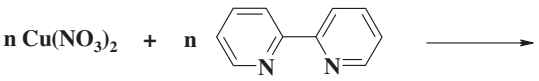

2,2'-Bipyridine

$$[Cu(NO_3)_2(C_{10}H_8N_2)]_n \qquad \text{(Reaction2)}$$

In the aforementioned examined systems, the isolated products **1** and **2** were crystalline and used as such for further spectroscopic and crystallographic studies. Elemental analyses on the derived products suggested the formulation $[Cu_2(CBTC)(H_2O)_4]{\cdot}2H_2O$ for **1** and $[Cu(NO_3)_2(bipy)]$ for **2**. Further X-ray crystallographic investigation confirmed the above analytical formulations in the respective coordination polymers.

Compounds **1** and **2** were stable in air for long periods of time and were insoluble in organic solvents. Compound **2** was soluble in water.

3.2. Description of the X-ray crystallographic structures

The three-dimensional X-ray structure determination of compound **1** revealed the presence of a molecular lattice with 16 molecules per unit cell. Selected interatomic distances and bond angles

Table 2
Bond lengths (Å) and angles (°) in **1** and **2**.

(**1**)		(**2**)	
Distances			
Cu–O(1)	1.908(2)	Cu–O(22)	1.958(2)
Cu–O(4′)	1.913(2)	Cu–O(13)	1.984(3)
Cu–O(6)	1.959(2)	Cu–N(2)	1.992(2)
Cu–O(5)	1.988(2)	Cu–N(1)	1.997(3)
Cu–O(3″)	2.397(2)	Cu–O(13′)	2.574(2)
		Cu–O(21″)	2.631(2)
Angles			
O(2)–Cu–O(4′)	176.70(7)	O(22)–Cu–O(13)	90.52(8)
O(2)–Cu–O(6)	91.98(7)	O(22)–Cu– N(2)	166.55(9)
O(4′)–Cu–O(6)	91.03(7)	O(13)–Cu– N(2)	96.96(8)
O(2)–Cu–O(5)	90.47(7)	O(22)–Cu– N(1)	89.12(7)
O(4′)–Cu–O(5)	86.29(7)	O(13)–Cu– N(1)	168.87(8)
O(6)–Cu–O(5)	166.96(8)	N(2)–Cu–N(1)	81.38(8)
O(2)–Cu–O(3″)	92.23(6)	O(13′)–Cu–O(21″)	176.16(7)
O(4′)–Cu–O(3″)	88.35(6)	O(22)–Cu–O(13′)	82.97(8)
O(6)–Cu–O(3″)	104.13(7)	O(13)–Cu–O(13′)	67.59(7)
O(5)–Cu–O(3″)	88.56(6)	N(1)–Cu–O(13′)	101.35(7)
		N(2)–Cu–O(13′)	89.54(8)
		O(22)–Cu–O(21″)	93.34(8)
		O(13)–Cu–O(21″)	111.49(7)
		N(1)–Cu–O(21″)	79.61(7)
		N(2)–Cu–O(21″)	94.27(8)

Symmetry transformations used to generate equivalent atoms:
1: (′) 0.75 − *y*, −0.75 + *x*, −0.75 + *z*; (″) 0.75 − *y*, −0.75 + *x*, 0.25 + *z*.
2: (′) −1 − *x*, 1 − *y*, 2 − *z*; (″) −*x*, 1 − *y*, 2 − *z*.

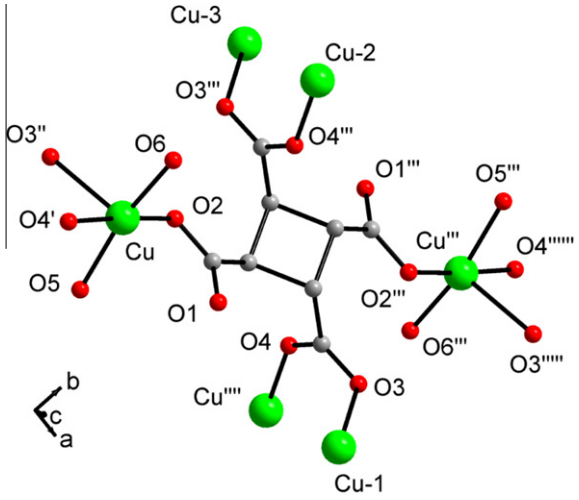

Fig. 1. Partially labeled plot of a small fragment of $[Cu_2(C_8H_4O_8)(H_2O)_4]_n{\cdot}2nH_2O$ (**1**) showing the binding of six Cu(II) ions through one tetracarboxylate ligand. Thermal ellipsoids represent 30% probability surfaces. Hydrogen atoms have been omitted for clarity. Symmetry operations: (′) 0.25 − *y*, −0.25 + *x*, 0.75 + *z*; (″) 0.25 − *y*, −0.25 + *x*, 0.25 + *z*; (‴) 0.5 − *x*, 0.5 − *y*, 0.5 − *z*; (⁗) 0.25 + *y*, 0.25 − *x*, −0.75 + *z*; (′⁗) 0.25 + *y*, 0.75 − *x*, −0.25 − *z*; (″⁗) 0.25 + *y*, 0.75 − *x*, −1.25 − *z*; (−1) 0.25 + *y*, 0.25 − *x*, 0.25 + *z*; (−2) 0.25 − *y*, 0.25 + *x*, 0.25 − *z*; (−3) 0.25 − *y*, 0.25 + *x*, 0.75 − *z*.

for **1** are listed in Table 2. Complex **1** crystallizes in the tetragonal space group $I4_1/a$. The asymmetric unit contains one Cu(II) ion, one half of a 1,2,3,4-cyclobutane-tetracarboxylate ligand, with the middle of the square ring residing on an inversion center, and three water molecules (Fig. 1). The Cu(II) ions adopt a tetragonal pyramidal geometry ($\tau = 0.16$) [13]. Each ion is coordinated by three carboxylate oxygen atoms (O(2), O(3″), and O(4′), respectively) from three different 1,2,3,4-cyclobutane-tetracarboxylate ligands ($CBTC^{4-}$) as well as two water molecules ((O(5) and O(6)). Therefore, the coordination sphere of Cu(II) is an all-oxygen donor atom sphere, created by two different types of ligands, namely the $CBTC^{4-}$ ligand and water. The basal plane of the tetragonal pyramid is defined by O(2), O(5), O(4′) and O(6). Specifically, the employed carboxylate ligand is fully deprotonated, with the overall charge of the ligand coordinated to Cu(II) being 4−. This charge is consistent with the ratio of one Cu(II) ion over half of the $CBTC^{4-}$ ligand in the asymmetric unit of the unit cell and the need for charge balance. The specific deprotonation mode of the polycarboxylic ligands towards the Cu(II) ion leads to the absence of any cations or anions in the lattice for balancing any arisen charge. Therefore, the inorganic bases employed in the synthesis were merely used to raise the pH of the reaction mixture, with no further involvement of their cations in the lattice.

The centrosymmetric ligand $CBTC^{4-}$ is bound to six discrete Cu(II) ions, with all of them being coordinated through the four carboxylate groups of the aforementioned ligand. In particular, the two diametrically opposed carboxylate moieties (O(2) and O(2‴)) of the $CBTC^{4-}$ ligand bind only one Cu(II) ion each in a monodentate fashion, in view of the fact that the second carboxylate oxygen atoms O(1) and O(1‴) are not involved in metal ion binding (Fig. 1). The interatomic distance between the Cu(II) ions bound by O(2) and O(2‴) [Cu and Cu‴] is 9.926(2) Å. Moreover, the other two diametrically opposed carboxylate moieties (O(3) and O(4), O(3‴) and O(4‴), respectively) bind two discrete Cu(II) ions each, thereby acting in a bidentate fashion. The interatomic distances between the Cu(II) ions bound by O(3)/O(4) and O(3‴)/O(4‴), Cu-1···Cu⁗ and Cu-2···Cu-3, respectively, are 4.761(2) Å, i.e. equal to the crystallographic *c* axis length. The distances between the Cu(II) ions bound by diametrically opposed bidentate carboxylate groups, i.e. Cu-1···Cu-2 and Cu-3···Cu⁗, are 8.269(2) Å. Therefore, the aforementioned link of six discrete Cu(II) ions with only one carboxylate binder is confirmed.

Through these links, a three dimensional channel structure is assembled. The asymmetric unit of this structure (with the exception of the water molecule containing the O(7) atom) is the building block of these channels. By applying symmetry operations in the space group $I4_1/a$ (origin choice 2), two types of channels form, as shown in Fig. 2A. The type-A channels form by applying the symmetry operation $[4^-(0,0,1/4)\ 1/4,0,z]$, a left-handed 4_1 symmetry axis parallel to the *c* axis and passing through the (1/4,0,0) point (this point lies in the middle of the channel indicated by A in Fig. 2A). The four Cu atoms generated (Cu, Cu-1, Cu-4 and Cu-5) in Fig. 2, form a left-handed helix with a pitch equal to the length of the crystallographic *c* axis. Within this channel, lattice host water molecules are located (those containing the O(7) atom), which also form a left-handed helix with the same pitch through O7–H7OB···O7 hydrogen bonds (Fig. 2A). The water helix is suspended in the walls of channel A through O7–H7OA···O1 hydrogen bonds. Type-B channels (indicated by letter B in Fig. 2A) form by applying the symmetry operation of a 4-fold roto-inversion parallel to the *c* axis and passing through the point (0,1/4,0) (middle of channels **B**), as shown in Fig. 2. The four Cu atoms (Cu, Cu-2, Cu-6 and Cu-7) in Fig. 2, comprising the walls of channel-B, form two interpenetrating ladders (Fig. 2B), which are related through S_4 symmetry. The rungs of the ladder are 7.525 Å long and the stiles are equal to the *c* axis length. In Fig. 2B, a side view of the two helices is also shown. Moreover, the relative arrangement of the channels in the unit cell is shown in Fig. 2C. The type-A channels are indicated as A and A′, because for symmetry reasons they are left handed (A) and right handed (A′), respectively. Both channels are assembled by 28-membered rings, which are parallel to the (1 1 0) plane, while each ring employs four discrete Cu(II) ions and four 1,2,3,4-cyclobutane-tetracarboxylate ligands. The Cu(II) ions are linked though formation of Cu–O–C–C–C–C–O–Cu chains (Fig. 2A). In addition to the differences based on symmetry considerations, channels A and B differ in their ability to host water molecules (O(7) atoms). This feature emerges mainly as a result of the

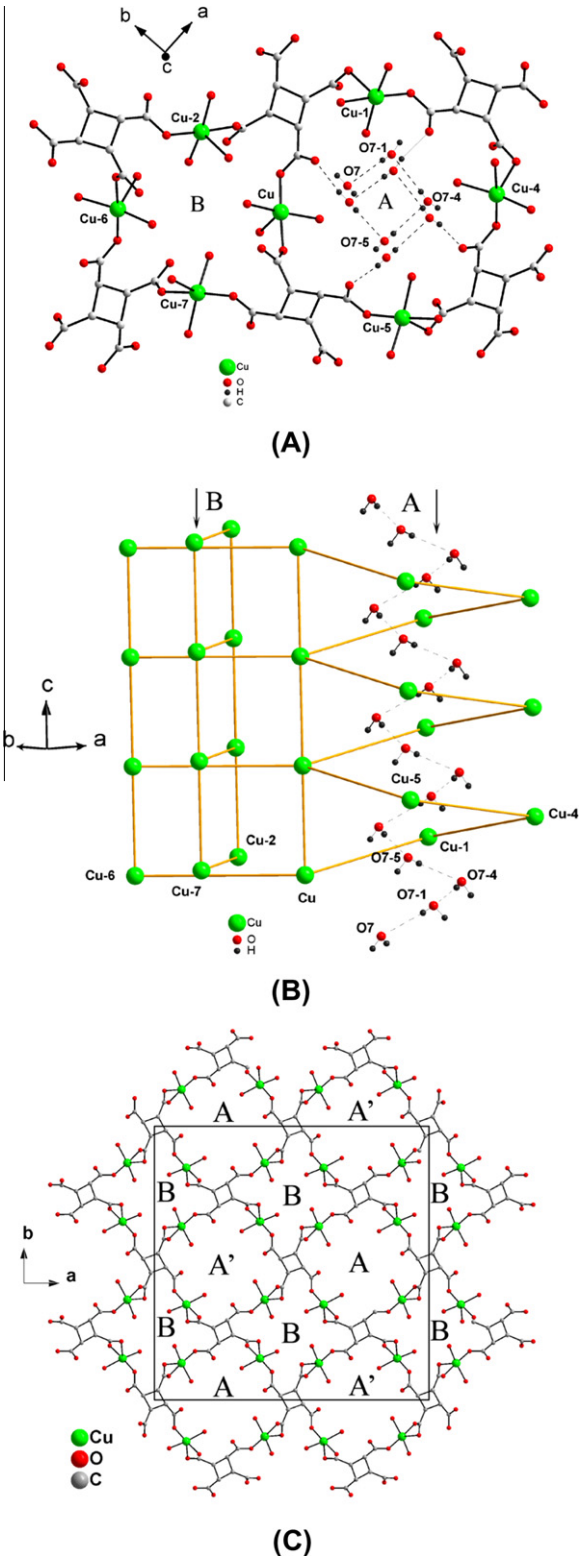

Fig. 2. (A) A small fragment of the 3D network of **1** looking down the *c* axis, showing the helical (A sites) and ladder type channels (B sites) described in the text. Within channels of type-A, the helix formed by water lattice molecules is also shown. Symmetry operations: (−4) 0.5 − *x*, −*y*, 0.5 + *z*; (−5) 0.25 − *y*, −0.5 + *x*, 0.75 + *z*; (−6) −x, 0.5 − *y*, *z*; (−7) −0.25 + *y*, 0.25 − *x*, 0.5 − *z*); (B) side view of helix (A) and ladder (B) type channels. Both of these building blocks of the 3D structure of **1** are constructed by translation along the *c* axis of the structure motif, shown in (A). Only the Cu(II) centers are shown for clarity. The development of the water molecule helix is also shown. (C) Arrangement of channels of type-A and type-B in the (001) crystallographic plane. A and A′ indicate sections of left-handed and right-handed helices, respectively.

difference in the diameter size of the two channels, which is 5.343 and 3.175 Å for the A (or A′) and B channels, correspondingly. To this end, the size and not the chemical environment primarily render channels A hydrophilic and B hydrophobic.

In conclusion, two reasons are responsible for the formation of the 3D structure of compound **1**: (a) the multifunctional nature of the employed 1,2,3,4-cyclobutane-tetracarboxylate ligand, and (b) the way the aforementioned ligand spans into the coordination sphere of the Cu(II) ions, binding six discrete metal ions in various coordination modes. To the best of our knowledge, a limited number of crystal structures containing the examined ligand have been reported so far. Representative examples of such complexes include $[Cd(C_8H_5O_8)(H_2O)_2]_n$ [14], $[La^{III}(C_8H_5O_8)]\cdot H_2O$ [15] and $[(U^{VI}O_2)_2(C_8H_4O_8)(H_2O)_2]\cdot 2H_2O$, $[(UO_2)_2(C_8H_4O_8)(H_2O)_2]\cdot H_2O$, and $[H_3O]_2[(UO_2)_5(C_8H_4O_8)_3(H_2O)_6]$ [16].

The Cu–O bond distances in **1** are in the range 1.908(2) to 2.397(2) Å and they are of a comparable length to those found in other Cu(II)–carboxylato complexes: $[Cu(C_4H_4O_5)(C_{10}H_8N_2)(H_2O)]$ (1.926(2)–2.468(2) Å) [17], $[Cu_3(C_9H_3O_6)_2(H_2O)_3(NH_3)_4]_n\cdot 2nH_2O$ (1.945(5)–2.790(8) Å) [18], $[Cu_4(C_9H_3O_6)_2(OH)_2(H_2O)_2(NH_3)_4]_n$ (1.926(2)–2.468(2) Å) [18]. In the organic–inorganic hybrid **1**, the copper ion exhibits a square pyramidal geometry, like various analogous Cu(II)-compounds reported in the literature: $[Cu_2(C_9H_9N_2O_3)(C_{10}H_8N_2)_2(OH_2)(OH)](NO_2)_2\cdot 4H_2O$ [19], $[Cu(C_5H_8NO_2)(C_{10}H_8N_2)_2(OH_2)](ClO_4)$ [19], $[Cu_2(C_7H_6N_2)_4(C_7H_{10}O_4)(C_7H_{11}O_4)_2\cdot 8H_2O]_n$ [20], $[Cu(2\text{-pc})(3\text{-pc})]_n$ [21], $[Cu(2\text{-pc})(4\text{-pc})]_n$ (pc=pyridine carboxylate) [21], $[Cu(C_6H_4NO_2)(C_6H_4NO_2)]_n$ [21], $[Cu_2(C_{12}H_{10}CO_2)_4(C_{12}H_{10}CO_2H)_2$ [22], $[Cu(C_6H_{10}NO_2)_2(H_2O)]$ [23], $\{[Cu(C_8H_4O_4)(C_{16}H_{20}N_4)(H_2O)]\cdot 5H_2O\}_n$ [24], $\{[Cu_2(C_{10}H_8O_4)_2(C_{16}H_{20}N_4)]\cdot H_2O\}_n$ [24] and $\{[Cu(C_{10}H_9O_4)(C_{16}H_{20}N_4)]\cdot(NO_3)\cdot 3H_2O\}_n$ [24].

Overall, the carboxylate ligand $CBTC^{4-}$ appears to play the role of an efficient metal ion binder, employing two types of binding modes and anchors (mode I and mode II in Scheme 1). Its ability to bind metal ions in different modes is supported by its multifunctional chemical structure, thus effectively formulating a diverse coordination environment around metal ions, such as encountered with Cd(II) [14] and La(III) [15]. As a result of the chemical composition and structural assembly, the lattice structure of **1** is stabilized by an extensive hydrogen bonding pattern (Fig. 2B and Table 3), contributing to a 3D network.

Compound **2** emerges from a molecular type of crystal lattice. The compound crystallizes in the triclinic system $P\bar{1}$ with two molecules per unit cell. The DIAMOND diagram of **2** is shown in Fig. 3. Selected interatomic distances and bond angles for **2** are listed in Table 2. The structure of **2** consists of a mononuclear core unit composed of an octahedral Cu(II) ion. The coordination sphere of Cu(II) consists of oxygen and nitrogen donor atoms, generated by two different types of ligands, namely, nitrate and 2,2′-bipyridine.

Specifically, one 2,2′-bipyridine molecule is coordinated to the metal ion through the two nitrogen atoms (N(1), N(2)). These two anchor atoms bind Cu(II) through the formation of a five-membered metallacyclic ring, rendering the arising species quite stable. In addition, two nitrate ions are coordinated to the Cu(II) ion through different binding modes. One nitrate ion employs a $\mu_2{:}\eta^1$ coordination mode and binds two neighboring Cu(II) ions through O(13) and its centrosymmetrically related atom (Scheme 2), thereby acting as a bridge. The second nitrate ion employs a $\mu_2{:}\eta^1{:}\eta^1$ coordination mode through O(21) and O(22) (Scheme 2), also bridging two neighboring Cu(II) ions. As a result, polymeric chains of Cu(1) assemblies form parallel to the crystallographic *a* axis (Fig. 4). The Cu···Cu distances through the $\mu_2{:}\eta^1$ nitrates are 3.802(2) Å, and those through the $\mu_2{:}\eta^1{:}\eta^1$ nitrates are 4.729(2) Å. The two different bridging modes adopted by the nitrates ions result in the formation of two different rings between two Cu(II) ions, the oxygen and the nitrogen atoms: (a) a

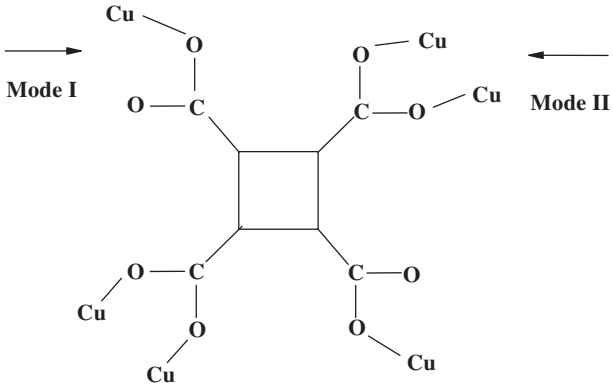

Scheme 1. Mode of metal–carboxylate coordination around the $CBTC^{4-}$ ligand.

Table 3
Hydrogen bonds in **1**.

Interaction	H···A (Å)	D···A (Å)	D–H···A (°)	Symmetry operation
O5–H5OA···O1	1.860	2.697	161.4	0.75 − *y*, −0.75 + *x*, 0.25 + *z*
O5–H5OB···O7	1.949	2.743	164.2	*x*, *y*, *z*
O6–H6OA···O3	2.064	2.841	159.5	2 − *x*, −*y*, 2 − *z*
O6–H6OB···O3	1.800	2.673	157.5	0.75 − *y*, −0.75 + *x*, −0.75 + *z*
O7–H7OA···O1	2.057	2.833	155.8	*x*, *y*, *z*
O7–H7OB···O7	2.111	2.863	168.6	0.75 − *y*, −0.75 + *x*, 0.25 + *z*

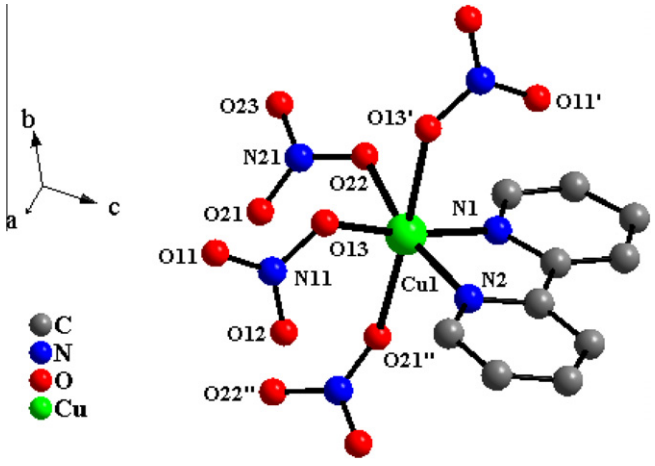

Fig. 3. Partially labeled plot of the mononuclear repeating unit in $[Cu(NO_3)_2(bipy)]_n$ (**2**). Thermal ellipsoids represent 30% probability surfaces. Hydrogen atoms have been omitted for clarity. Symmetry operations: (′) −1 − *x*, 1 − *y*, 2 − *z*; (″) −*x*, 1 − *y*, 2 − *z*.

four-membered ring defined by Cu–O–Cu–O, with the covered area being 5.106 Å^2, and (b) an eight-membered ring defined by Cu–O–N–O–Cu–O–N–O. The four-membered Cu_2O_2 rings form contiguously with the eight-membered rings along the crystallographic *a* axis, with the different bridging modes between adjacently located Cu(II) ions in each ring affecting the Cu···Cu separation distance.

The octahedron around each Cu(II) ion is defined by the oxygen atoms O(13) and O(22) and the nitrogen atoms N(1) and N(2) in the equatorial plane, whereas the remaining two atoms, O(13′) and O(21″), occupy the axial positions. Careful examination of

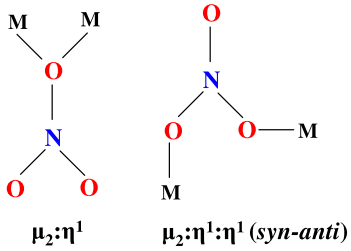

Scheme 2. Metal–nitrate binding modes in **2**.

the Cu–O distances in **2** reveals a distinct distortion of the octahedron around Cu(II). It appears that two of the Cu–O bond distances (Cu–O(13′) 2.574(2) Å, Cu–O(21″) 2.631(2) Å) are considerably longer than the other four (1.958(2)–1.997(2) Å), with the latter bonds formulating the equatorial environment of the octahedral metal ion. The stark bond length differentiation between the former bonds (axial) and the other four bonds (equatorial) exemplify a tetragonal elongation that the octahedral complex undergoes as a result of a Jahn–Teller distortion. Consistent with the presence of a Jahn–Teller distortion in a d^9 metal ion, the tetragonality factor $T = R_S/R_L$, where R_S is the mean in-plane copper–ligand bond length and R_L is the mean out-of plane (axial) bond length, appears to be 0.76 [25]. A *T* value smaller than 1 (regular octahedron, $T = 1$) indicates the presence of a tetragonally distorted octahedron.

A number of Cu(II)–(2,2′-bipyridine) and Cu(II)–(2,2′-bipyridine-derivatives) have been isolated and characterized, with five or six coordinate Cu(II) ions: $[\mu\text{-}(C_2O_4)\{Cu(C_{11}H_{12}N_2)(NO_3)(H_2O)\}_2]$ [26], $[\mu\text{-}(C_2O_4)\{Cu(C_{11}H_{12}N_2)(ClO_4)(H_2O)\}_2]$ [26], $[Cu(\text{-}C_6H_8O_8)(C_{10}H_8N_2)]_n{\cdot}2nH_2O$ [27], $[Cu(NO_3)_2(C_{16}H_{10}N_4)]$ [28], $Cu(\text{-}C_8H_{10}O_2F_3)_2(C_{12}H_8N_2)$ [29], $Cu(C_8H_{10}O_2F_3)_2(C_{10}H_8N_2)$ [29] and $[Cu(NO_3)_2(C_{18}H_{24}N_2)]$ [30].

3.3. Electronic spectroscopy

The UV–Vis spectrum of **2** was recorded in water (see Supporting Information). The spectrum exhibits a major peak at $\lambda_{max} = 697$ nm ($\varepsilon \sim 38\ M^{-1}\ cm^{-1}$), and a strongly absorbing band rising into the UV region with a maximum at 310 nm ($\varepsilon \sim 1422\ M^{-1}\ cm^{-1}$). The absorption feature in the low energy region can be attributed to *d*–*d* transitions, which are typical for a Cu(II) d^9 tetragonally distorted octahedral species. To this end, the band at 697 nm, displaying a broad absorption envelope, likely encompasses $d_{xy} \rightarrow d_{x^2-y^2}$ and $(d_{xz}, d_{yz}) \rightarrow d_{x^2-y^2}$ transitions. The observed pattern is in line with the Jahn–Teller effect acting on the ^2E_g ground term of the d^9 octahedron [31], leading to a tetragonal distortion of the complex along the interligand axis. The latter feature likely belongs to a LMCT band in the UV region. In the absence of detailed studies, no further assignments could be proposed. The spectrum of **2** in water is different from that of $Cu(II)_{aq}$ [32], reflecting the unique coordination sphere composition of Cu(II) in solution.

3.4. Infrared spectroscopy

The FT-infrared spectra of **1** and **2** were recorded in KBr. In **1**, the spectrum reveals the presence of resonances attributed to vibrationally active carbonyls of the carboxylate ligand. The antisymmetric stretching vibrations $\nu_{as}(COO^-)$ appear between 1565 and 1517 cm^{-1}. The symmetric stretching vibrations $\nu_s(COO^-)$ appear at 1410 cm^{-1}. The frequencies of the aforementioned bands are shifted to lower values compared to the corresponding vibrations in 1,2,3,4-cyclobutane-tetracarboxylic acid, thus indicating a change in the metal ion coordination status with the carboxylates in the aforementioned ligand. The frequency difference,

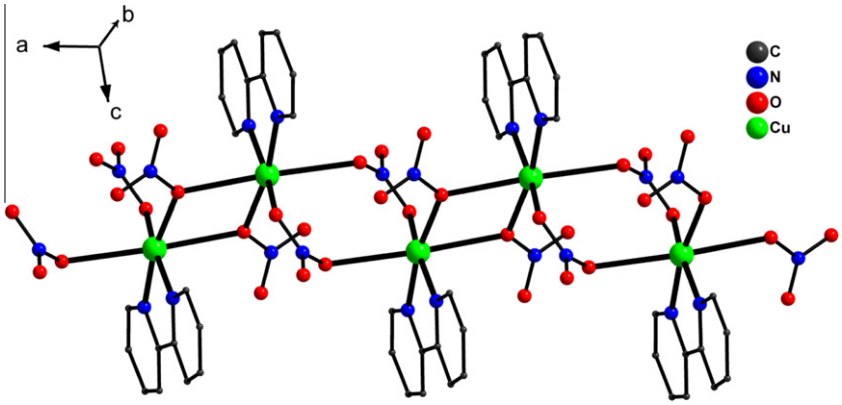

Fig. 4. A small fragment of the 1D chain of **2** extending parallel to the crystallographic *a* axis.

$\Delta(\nu_{as}(COO^-)-\nu_s(COO^-))$ [33,34], in **1** is greater than 200 cm^{-1}, indicating the presence of deprotonated carboxylate groups coordinated to the metal ion in a monodentate fashion. This assertion is further proven by the X-ray crystal structure determination of **1**. In **2**, the bands that appear between 3040 and 3120 cm^{-1} suggest the presence of 2,2′-bipyridine, and they are shifted compared to the free 2,2′-bipyridine, indicating changes in the vibrational status of the ligand due to the bidentate coordination of the N atoms to the Cu(II) ions. The aforementioned assignments are in agreement with previously reported 2,2′-bipyridine complexes with various metal ions [35–37]. Furthermore, the NO_3^- groups exhibit absorptions bands that differ beyond the coordination mode in each compound. In **2**, the NO_3^- groups are coordinated to copper ions both in a monodentate and bidentate fashion. The NO_3^- groups that are coordinated in a monodentate fashion exhibit absorptions bands at 1312 and 1442 cm^{-1}, whereas the NO_3^- groups coordinated in a bidentate fashion exhibit absorptions bands at 1473 and 807 cm^{-1} [38].

3.5. Thermogravimetric studies

The thermal decomposition of both **1** and **2** was studied by TGA–DTG under an atmosphere of oxygen (see Supporting Information). The TGA diagram shows that the initial process involves a total loss of water molecules per formula unit of **1**. The release of water molecules is observed as expected in the first phase of the process. An additional step is observed that involves the decomposition of the organic moiety bound to Cu(II). The thermal dissociation of **1** signifies an exothermic process [39]. The total weight loss of complex **1** is close to 66.5% and is reached at approximately 374 °C. No further decomposition occurs beyond that temperature and until a final temperature of 700 °C. The final product corresponds to CuO [40–42]. The small number of observed TGA peaks suggests simple mechanisms of decomposition for **1**.

In a similar fashion, the TGA diagram of **2** shows a quite simple process reflecting the weight loss of **2**. The decomposition of **2** shows an exothermic process associated with the specific chemical nature of compound **2**. The total weight loss due to the decomposition of **2** is 82.4% and is reached at approximately 285 °C. No further changes are observed beyond that temperature and up to the final temperature of 700 °C. The nature of the derived solid product of the thermal decomposition conforms with the formation of the metal oxide [43].

3.6. Cyclic voltammetry

The cyclic voltammetry of compound **2** was studied in aqueous solution, in the presence of KNO_3 as a supporting electrolyte (Fig. 5). The cyclic voltammogram projects a well-defined electrochemical behavior, with a pronounced chemically reversible process reflected in: (a) a reduction wave at E_{pc} −172.6 mV, and (b) an oxidation wave at E_{pa} 0.892 mV, and (c) a value of $E_{1/2}$ of −85.9 mV ($i_{pc}/\{(v)^{1/2}C\}$ constant and $i_{pa}/i_{pc} = 1$). Therefore, the observed chemically reversible redox wave likely corresponds to the redox Cu(II)/Cu(I) couple [44]. Attempts to pursue the redox chemistry of compound **2** are currently ongoing.

3.7. Luminescence

Copper complexes containing heterocyclic aromatic ligands have been reported to exhibit interesting luminescence properties, with emission bands arising in the range from 400 to 600 nm [44–46]. The luminescence properties of the isolated compound **2** and the free ligand 2,2′-bipyridine were investigated in methanol and at room temperature. The concentration of **2** and the free ligand was 10^{-5} M. The excitation and emission spectra of compound **2** and the free ligand are shown in Fig. 6. Compound **2** and the free ligand exhibit an emission band at 416 nm. Coordination of the ligand to the metal ion increases the rigidity of the molecular edifice and increases the loss of energy through radiationless thermal vibrations [47,48]. Thus, what one observes is a decrease in the intensity of both the excitation and the emission signal of complex relative to the ligand [49]. The band located at 416 nm in the emission spectrum of complex **2** is most probably due to a π–π^* transition of the 2,2-bipyridine ligand [50,51].

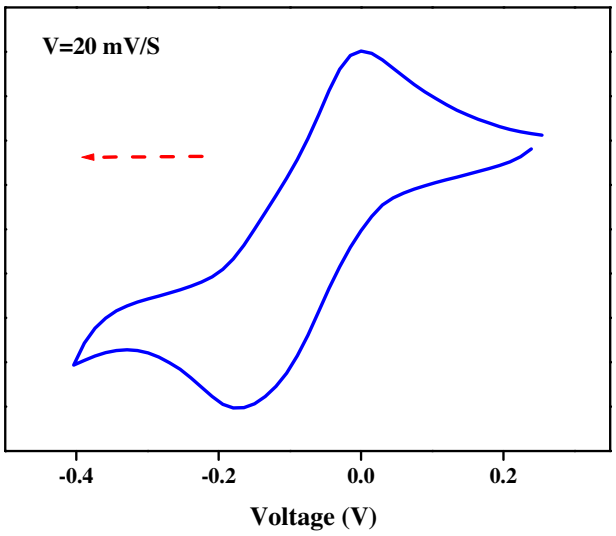

Fig. 5. Cyclic voltammetry of compound **2** in aqueous solution (scan rate 20 mV/s).

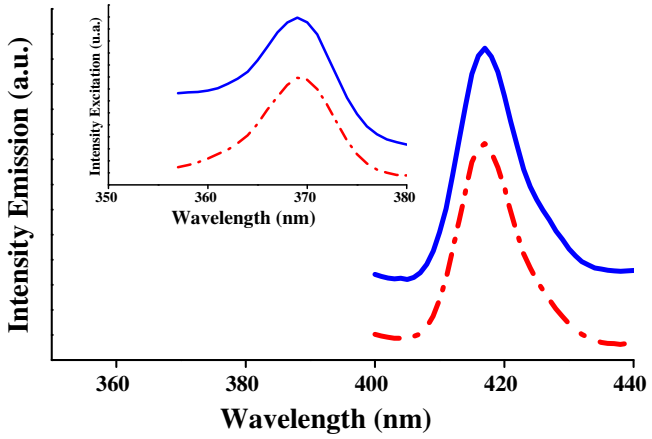

Fig. 6. Solution emission spectrum of compound **2** (red line) and free 2,2′-bipyridine (blue line) in methanol. Inset: Solution excitation spectrum of compound **2** and free 2,2′-bipyridine (blue line) in methanol. (For interpretation of the references to color in this figure legend, the reader is referred to the web version of this article.)

3.8. Magnetic susceptibility

Magnetic susceptibility measurements were carried out at different magnetic fields and in the temperature range 2–300 K. Fig. 7 shows the $\chi_M T$ versus T susceptibility data at 0.5 T for compound **1**, while Fig. 8 shows the $\chi_M T$ (per 2 Cu(II) ions) versus T susceptibility behavior for compound **2**.

The $\chi_M T$ values decrease almost linearly from 1.42 emu mol^{-1} K (**1**) and 0.88 emu mol^{-1} K (**2**) at 300 K to 0.89 emu mol^{-1} K (**1**) and 0.65 emu mol^{-1} K at 18 K (**2**), and then more steeply to the values of 0.65 emu mol^{-1} K at 2.0 K (**1**) and 0.58 emu mol^{-1} K at 2.0 K (**2**). The temperature independent paramagnetism, TIP, is responsible for the linear-like behavior of $\chi_M T$, while the abrupt decrease of the susceptibility data in the low temperature range is due to small interdinuclear antiferromagnetic interactions.

A simplified spin Hamiltonian model (based on crystallographic criteria) was used to describe the exchange interaction in compound **1** and is shown in Eq. (1). According to this model, weakly interacting dimers are connected, giving rise to a complex 3D structure. In order to take into consideration the weak inter-dimer interactions, a mean field correction term was added to the isotropic spin exchange term.

$$H = -2J(\mathbf{S}_1\mathbf{S}_2) - zJ'\langle S_z\rangle S_z + g\beta H\mathbf{S} \quad (1)$$

Two possible sets of values for the fitted parameters were found, giving identical results (solid line in Fig. 7): (a) $J = -0.53$ cm^{-1}, $g = 2.16(1)$, TIP = 1.8×10^{-3} and (b) $J = -0.43$ cm^{-1}, $zJ = -0.23$, $g = 2.16(1)$, TIP = 1.8×10^{-3}. Further magnetization measurements (see below) are expected to elucidate the significance of the interdimer interaction.

In the case of compound **2**, two different models were employed to derive the exchange interactions. In the first model (according to crystallographic criteria), the repeating unit is a dimer and a mean field correction was applied for the inter-dimer interactions (Eq. (1)). Two possible sets of values for the fitted parameters were found, giving identical results (solid line in Fig. 8): (a) $J = -0.23$ cm^{-1}, $g = 2.1(1)$, TIP = 7.7×10^{-4} and (b) $J = -0.11$ cm^{-1}, $zJ = -0.15$, $g = 2.1(1)$, TIP = 7.7×10^{-4}. The role of the inter-dimer parameter is further elucidated through magnetization studies. The second model used is the Bonner–Fisher model [52] (Eq. (2)) for a uniformly spaced chain of $S = 1/2$ metal centers. Since the two different exchange pathways are expected to give rise to small

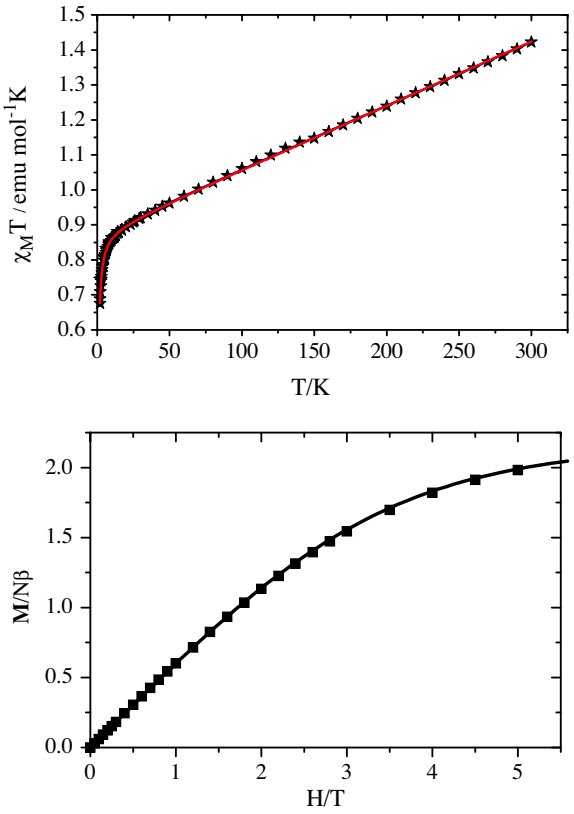

Fig. 7. (Top) Temperature dependence of the magnetic susceptibility of **1**, in the form of $\chi_M T$ vs. T, in the temperature range 2–300 K, in the presence of an external magnetic field of 0.5 T. The solid line represents the fitting results (see text). (Bottom) Magnetization of **1**, in the form of $M/N\mu_B$ vs. H/T, at 2 K and in the field range 0–5 T. The solid line represents the simulation according to the susceptibility fitting results (see text).

antiferromagnetic interactions, this model likely projects a good approximation.

$$\chi = \frac{Ng^2\beta^2}{kT}\frac{0.25 + 0.07497x + 0.075235x^2}{1.0 + 0.9931x + 0.172135x^2 + 0.757825x^3} \quad (2)$$

where $x = \frac{|J|}{kT}$.

The fit (identical solid line in Fig. 8) gave $|J| = 0.1$ cm^{-1}, $g = 2.1(1)$, and TIP = 4×10^{-4}, with the values obtained being close to the second set of the first model.

3.9. Magnetization studies

The magnetization data for **1** and **2** in the form of $M/N\mu_B$ versus H/T at 2 K and in the field range 0–5 T are shown in Figs. 7 and 8, respectively (for compound **2** the data are per 2 Cu(II) ions).

In the case of compound **1**, simulations of the magnetization data were performed using the same model (Eq. (1)) and the obtained sets of parameters described in the previous section. The results are shown as a solid line superimposable to the experimental curves in the case of the first set of parameters [$J = -0.53$ cm^{-1}, $g = 2.16(1)$], thereby verifying that there is an almost zero inter-dimer interaction. A different situation emerges for compound **2**, where simulation of the magnetization curve using the first set of parameters [$J = -0.23$ cm^{-1}, $g = 2.1(1)$], presented as solid stars in the magnetization data of Fig. 8, diverges significantly from the experimental data, thus denoting the importance of the inter-dimer interactions.

A different magnetic model was used in order to simulate the magnetization curve of compound **2** and is shown in (Eq. (3)):

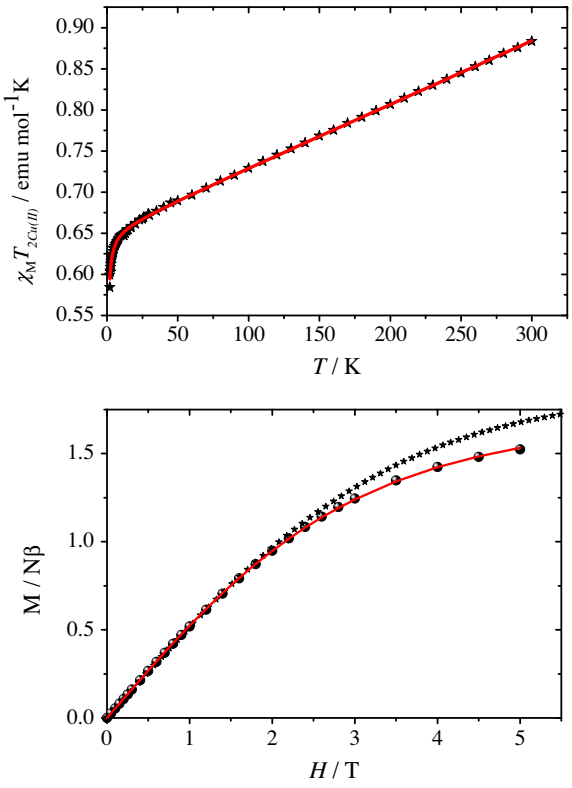

Fig. 8. (Top) Temperature dependence of the magnetic susceptibility of **2**, in the form of $\chi_M T$ vs. T, in the temperature range 2–300 K, in the presence of an external magnetic field of 0.5 T. The solid line represents the fitting results according to the Hamiltonian models described in Eqs. (1) and (2) (see text). (Bottom) Magnetization of **2**, in the form of $M/N\mu_B$ vs. H/T, at 2 K and in the field range 0–5 T. The solid stars represent the simulation according to the susceptibility fitting results (see text), while the solid line represents the fitting results according to the Hamiltonian model described in Eq. (3) (see text).

$$H = g\beta HS_z + zJ'\langle S_z\rangle S_z \tag{3}$$

where Cu(II) ions, bearing $S = 1/2$, (a) are weakly interacting, (b) the magnetic field is assumed to be along the z direction, and (c) the g-tensor is taken to be isotropic. $\langle S_z\rangle$ is given by the Boltzmann distribution law:

$$\langle S_z\rangle = \frac{\sum_{M_S=-S}^{S} M_S \exp[-E(S,M_S)/kT]}{\sum_{M_S=-S}^{S} \exp[-E(S,M_S)/kT]} = \frac{\sum_{M_S=-S}^{S} M_S \exp[1 - M_S(g\mu_B H - zJ\langle S_z\rangle)/kT]}{\sum_{M_S=-S}^{S} \exp[1 - M_S(g\mu_B H - zJ\langle S_z\rangle)/kT]} \tag{4}$$

According to Eqs. (3) and (4) the magnetization formula becomes

$$M = -Ng\mu_B\langle S_z\rangle \tag{5}$$

Assuming that the zJ is non-zero, a perfect fit appears and the fitting results are $g/zJ' = (2.1(1)/0.2(1)\ \mathrm{cm}^{-1})$. Although the values obtained for the mean field correction are large, both the susceptibility and magnetization models draw a clear trend of the importance of this exchange interaction.

3.10. EPR spectroscopy

X-band EPR measurements were carried out on **1** and **2**, in the powder form, at 4 K. In both cases, almost isotropic spectra (see Supporting Information) emerged for the powder samples, with features centered at 2.16(1) and 2.15(1), respectively. The signals obtained are characteristic of high spin Cu(II) signals in consonance with the results of the fitting procedures of the aforementioned magnetic data.

4. Discussion

4.1. The synthetic chemistry interplay of binary and ternary Cu(II)–ligand systems

The interaction between transition metal ions, such as Cu(II), and various carboxylate-bearing ligands has been a challenge in research over the past few years. Studies between Cu(II) ions and diversely structured carboxylic substrates have been carried out and are currently providing useful information on how chemical reactivity in binary and/or ternary systems is linked to the emergence of lattice specific structures (1D-, 2D-, 3D-dimensional coordination polymers) with distinct properties leading to promising functional materials [53]. As an important family of multidentate O-donor ligands, tetracarboxylic acids have been under investigation for their chemical reactivity towards transition metal ions [54]. H_4CBTC is such a ligand, which possesses the following structural features: (a) it is a cyclic aliphatic carboxylic acid-containing ligand structured so as to provide metal anchors around its periphery, and (b) it contains four carboxylic acid moieties positioned symmetrically around the cyclic skeleton of the ligand, thereby providing ample access to binding metal ions leading to Cu(II)–organic hybrid compounds with a plethora of compositions, lattice architectures and dimensionality options. In this regard, the pH-specific reactivity of $CuSO_4$ toward H_4CBTC exemplifies the mutual chemical affinity and the diversity of the observed binding modes. Undoubtedly, the pH of the reaction solutions employed in this work was crucial in investigating the reactivity. Furthermore, the analytical and spectroscopic characterization of the derived organic–inorganic hybrid materials reflected the physical and chemical properties of **1** and **2**, and revealed a considerable number of structural details related to metal–(O,N) ligand materials. To this end, the electronic, vibrational, electrochemical (where applicable), magnetic and EPR properties formulated the profile of the two coordination polymers and projected their distinct structures in the solid state and in solution.

4.2. From chemical reactivity attributes to lattice architecture

Compound **1** provides the first example of a Cu(II)–(1,2,3,4-cyclobutanetetracarboxylato) binary compound among other well-characterized Cu(II)–carboxylato species with the following unique properties: (a) the four carboxylate groups of the aforementioned ligand bind six discrete Cu(II) ions in variable denticity modes, (b) two of the four carboxylate moieties have one oxygen anchor not coordinated to copper ions, (c) the copper ions are five coordinate, exhibiting square pyramidal geometries. Amply shown through X-ray crystallography, two of the four carboxylates (located at diametrically opposed sites around the cyclobutane ring) bind one Cu(II) center in a monodentate fashion, thereby differentiating their chemical reactivity from the remaining two carboxylates, each of which binds two Cu(II) ions (Scheme 1). This selectivity in the chemical reactivity of the carboxylates around the cyclobutane ring may be a consequence of the spatial requirements of single versus double metal ion coordination on behalf of each carboxylate group and influences heavily the composition as well as the nature of the ultimately assembled lattice. It has been well-known that carboxylate groups are capable of coordinating metal ions in diverse ways, with the employed metal coordination modes influencing the nature of the emerging metal–organic hybrid crystal lattice. In the aforementioned binary system, the interaction of Cu(II) ions with H_4CBTC distinctly led to an assembly,

exemplified through the binding of each of the four carboxylate moieties to the Cu(II) ions in a monodentate and/or bidentate fashion [55]. Undoubtedly, the structurally revealed composition of the unit $Cu_2(C_8H_4O_8)(H_2O)_4$ supports the ligand associated extension into the 3D polymeric lattice, in keeping with the requirements of the composition and the properties of the derived crystalline product **1**. What is unique about the lattice structure of **1** is that there exist two types of channels (A and B) with unique characteristics. Specifically, both types of channels (a) are characterized by well-defined helices structurally supported by Cu(II) centers bound to the deprotonated ligand, and (b) have the same helical pitch, i.e. that covering the length of the crystallographic *c* axis. Surprisingly, type A channels contain – almost homocentrically – left-handed helices comprised of water molecules, with the helices linked to the outer Cu-supported walls through H-bonds. To this end, the type A channels differ from the type B channels in their nature, and diameter size (vide supra), and in so doing they exhibit a different capacity for "holding within" water molecules. The differentiated structural lattice helices A and B within the same lattice emerge as differentiated hosts for water molecules, with the latter capacity amply reflected in their hydrophilic/hydrophobic potential.

Delving further into the chemical reactivity of the ternary Cu(II)–H_4CBTC–(2,2′-bipy) system, the synthetic process led to the binary species **2**, not incorporating the H_4CBTC ligand into its lattice. Compound **2** represents a 1D lattice where nitrate ions and 2,2′-bipyridine fulfill the requirements of the coordination sphere of Cu(II). The nitrate ions are coordinated to Cu(II) ions via two discrete ways. In the first mode the nitrate ions act as $\mu_2{:}\eta^1$ bridging ligands (Scheme 2). Examples of compounds where one oxygen atom of a nitrate group bridges two metal ions are rare, although this bridging mode has been previously reported [56–58]. In **2**, the Cu–O–Cu bridges are asymmetric (Cu–O 1.984(3) and 2.574(2) Å) and the difference in length between the two Cu–O bonds is equal to 0.59 Å. This difference is in the range 0.2–0.7 Å, supporting this type of bridging for the nitrate group [59]. However, symmetrical Cu–O–Cu bridges have also been reported [60]. The second mode of coordination is $\mu^2{:}\eta^1{:}\eta^1$, as a *syn–anti* bidentate bridge (Scheme 2), similar to the bridging mode of carboxylates [61]. An important feature of the structure in **2** is the dihedral angle (δ) observed between the least-squares planes through the bridging nitrates. The angle δ between the planes O(21)–N(21)–O(22) and O(22)–O(21)–Cu(1) is 81.17° and the corresponding angle between the planes O(21)–N(21)–O(22) and O(22)–O(21)–Cu(1) is 178.46° (Scheme 3). Moreover, the Cu–O distances are unequal and the difference is 0.67 Å. Therefore, the role of the nitrate ions is to serve as pincer ligands, aiding in the assembly of a 1D lattice architecture in **2**. It is this diversity in the bridging mode of the nitrate ions that allows for the extension of the unit $Cu(NO_3)_2(C_{10}H_8N_2)$ into the one-dimensional coordination polymer **2** and the distinct properties tied to its lattice architecture.

With both Cu(II) and H_4CBTC being common partners at the binary and ternary level, key structural features of H_4CBTC were crucial in dictating the reactivity observed, with the third partner 2,2′-bipy dictating effectively the presence/absence of H_4CBTC from the isolated product of the ternary system (and consequently defining a new lattice composition, architecture and properties).

5. Conclusions

The synthetic chemistry of the binary Cu(II)–(1,2,3,4-cyclobutane-tetracarboxylic acid) system and its ternary congener with 2,2′-bipy led to well-defined materials **1** and **2**, the structural and spectroscopic properties of which exemplified the distinct chemical reactivity of each system and key features of their coordination

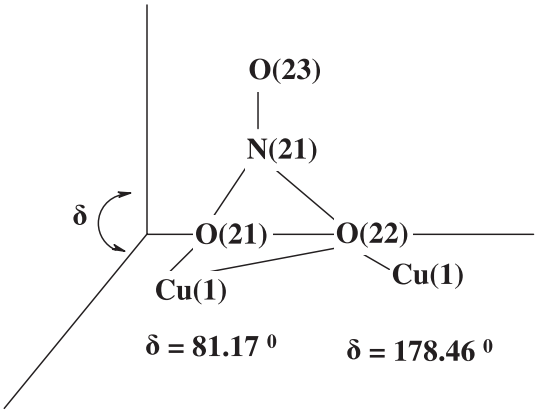

Scheme 3. The dihedral angle (δ) between the two planes defines the *syn–anti* coordination mode of the nitrate ions in **2**.

polymeric lattices. The physicochemical attributes of the coordination polymeric species **1** and **2** reflect the chemical diversity of the aforementioned reaction systems in aqueous media and indicate a complex structural speciation as a function of pH and molecular stoichiometry. The distinct structural and magnetic properties of the two polymeric materials (a) exemplify the unique nature of their solid state lattice composition, (b) emphasize the emergence of structurally differentiated domains (helical type A sites and interpenetrating ladder type B channels) within the unique Cu–ligand assembly as a result of the variable metal–ligand binding modes [the latter reveal distinct sub-structures (size, hydrophilicity/hydrophobicity, and thus water capacity differentiated left-handed helical channels in **1**, *syn–anti* conformationally distinct Cu–nitrate unidimensional chains in **2**) emerging within the lattice architecture of each coordination polymer] and (c) point towards the nature and chemical reactivity of the interacting ligand in the assembly as key factors influencing the magnetically active inorganic–organic polymeric materials of variable dimensionality (1D–3D). Efforts to unravel novel Cu(II)–(O,N-containing) coordination polymers through the employment of novel diversely structured (poly)carboxylic acids, capable of influencing the emergence of structurally and magnetically unique lattice architectures of variable yet well-defined dimensionality, as well as correlations thereof, are currently being pursued in our lab.

Acknowledgment

This research has been co-financed by the EU–ESF and Greek national funds through the NSRF-Heracleitus II program.

Appendix A. Supplementary data

CCDC 837646 and 837647 contain the supplementary crystallographic data for **1** and **2**, respectively. These data can be obtained free of charge via http://www.ccdc.cam.ac.uk/conts/retrieving.html, or from the Cambridge Crystallographic Data Centre, 12 Union Road, Cambridge CB2 1EZ, UK; fax: (+44) 1223-336-033; or e-mail: deposit@ccdc.cam.ac.uk. Supplementary data associated with this article can be found, in the online version, at http://dx.doi.org/10.1016/j.poly.2012.04.012.

References

[1] H. Tapiero, D.M. Townsend, K.D. Tew, Biomed. Pharmacother. 57 (2003) 386.
[2] L.J.C. Jeuken, M. Ubbink, J.H.B. Pieter van Vliet, W. Meyer-Klaucke, G.W. Canters, J. Mol. Biol. 299 (2000) 737.
[3] E.L. Gross, G.P. Anderson, S.L. Ketchner, J.E. Draheim, Biochem. Biophys. Acta 808 (1985) 437.

[4] P. Deschamps, P.P. Kulkarni, M. Gautam-Basak, B. Sarkar, Coord. Chem. Rev. 249 (2005) 895.
[5] J.H. Menkes, Eur. J. Paediatr. Neurol. 3 (1999) 147.
[6] V. Medici, L. Rossaro, G.C. Sturniolo, Dig. Liver Dis. 39 (2007) 601.
[7] Y. Wei, K. Wu, R. Broer, B. Zhuang, Y. Yu, Inorg. Chem. Commun. 10 (2007) 910.
[8] J. Moncol, P. Segla, D. Miklos, M. Mazur, M. Melnik, T. Glowiak, M. Valko, M. Koman, Polyhedron 25 (2006) 1561.
[9] A. Aijaz, E.C. Sanudo, P.K. Bharadwaj, Inorg. Chim. Acta 362 (2009) 4246.
[10] Rigaku/MSC CRYSTALCLEAR, Rigaku/MSC Inc., The Woodlands, Texas, USA, 2005.
[11] G.M. Sheldrick, SHELXS-97: Structure Solving Program, University of Göttingen, Göttingen, Germany, 1997.
[12] G.M. Sheldrick, SHELXL-97: Crystal Structure Refinement, University of Göttingen, Göttingen, Germany, 1993–7.
[13] A.W. Addison, T.N. Rao, J. Reedijk, J. van Rijn, G.C. Verschoor, J. Chem. Soc., Dalton Trans. (1984) 1349.
[14] J. Luo, F. Jiang, R. Wang, M. Hong, Inorg. Chem. Commun. 7 (2004) 638.
[15] Y.J. Kim, D.-Y. Jung, Inorg. Chim. Acta 338 (2002) 229.
[16] P. Thuéry, B. Masci, Cryst. Growth Des. 8 (2008) 3430.
[17] L. He, Acta Crystallogr., Sect. E 61 (2005) m1752.
[18] W.-X. Chen, S.-T. Wu, L.-S. Long, R.-B. Huang, L.-S. Zheng, Cryst. Growth Des. 7 (2007) 1171.
[19] P. Sgarabotto, F. Bisceglie, G. Pelosi, L. Abdel-Rahman, Polyhedron 18 (1999) 2505.
[20] G.A. Van Albada, J.G. Haasnoot, J. Reedijk, M. Biagini-Cingi, A.M. Manotti-Lanfredi, F. Ugozzoli, Polyhedron 14 (1995) 2467.
[21] S. Zhang, Y. Cao, H. Zhang, X. Chai, Y. Chen, J. Solid State Chem. 181 (2008) 399.
[22] T.C.W. Mak, W.-H. Yip, C.H.L. Kennard, G. Smith, Polyhedron 9 (1990) 1667.
[23] Y. Inomata, M. Ando, F.S. Howell, J. Mol. Struct. 616 (2002) 201.
[24] L. Johnston, J.H. Nettleman, M.A. Braverman, L.K. Sposato, R.M. Supkowski, R.L. LaDuca, Polyhedron 29 (2010) 303.
[25] (a) B.J. Hathaway, A.A.G. Tomlinson, Coord. Chem. Rev. 5 (1970) 1;
(b) B.J. Hathaway, D.E. Billing, Coord. Chem. Rev. 5 (1970) 143;
(c) B.J. Hathaway, Struct. Bond. 14 (1973) 49.
[26] D.M. de Faria, M.I. Yoshida, C.B. Pinheiro, K.J. Guedes, K. Krambrock, R. Diniz, L.F.C. de Oliveira, F.C. Machado, Polyhedron 26 (2007) 4525.
[27] M. Saladini, M. Candini, D. Iacopino, L. Menabue, Inorg. Chim. Acta 292 (1999) 189.
[28] C.M. Fitchett, P.J. Steel, Polyhedron 26 (2007) 400.
[29] O.Y. Gorbenko, S.I. Troyanov, A. Meetsma, A.A. Bosak, Polyhedron 16 (1997) 1999.
[30] X. Xiao, Z.-Y. Rao, Y.-Q. Zhang, S.-F. Xuea, Z. Tao, Acta Crystallogr., Sect. E 65 (2009) m202.
[31] A.B.P. Lever, Inorganic Electronic Spectroscopy, second ed., Elsevier, Amsterdam, 1984.
[32] (a) B.N. Figgis, Introduction to Ligand Fields, Interscience Publishers, New York, 1966;
(b) C.K. Jorgensen, Adv. Chem. Phys. 5 (1963) 33;
(c) C.J. Ballhausen, Introduction to Ligand Field Theory, McGraw-Hill Book Co., New York, 1962.
[33] C. Djordjevic, M. Lee, E. Sinn, Inorg. Chem. 28 (1989) 719.
[34] G.B. Deacon, R. Philips, J. Coord. Chem. Rev. 33 (1980) 227.
[35] S. Sen, S. Mitra, P. Kundu, M.K. Saha, C. Krtiger, J. Bruckmann, Polyhedron 16 (1997) 2475.
[36] E. Guney, V.T. Yilmaz, C. Kazak, Polyhedron 29 (2010) 1285.
[37] L. Tian, N. Ren, J.-J. Zhang, H.-M. Liu, J.-H. Bai, H.-M. Ye, S.-J. Sun, Inorg. Chim. Acta 362 (2009) 3388.
[38] K. Nakamoto, Infrared Spectra of Inorganic and Coordination Compounds, Wiley and Sons, New York, 1963.
[39] T.M. Southern, W.W. Wendlandt, J. Inorg. Nucl. Chem. 32 (1970) 3783.
[40] A.T. Çolak, F. Çolak, D. Akduman, O.Z. Yeşilel, O. Büyükgüngör, Solid State Sci. 11 (2009) 1908.
[41] W.M. Keely, H.W. Maynor, J. Chem. Eng. Data 8 (1963) 297.
[42] J. Ghose, A. Kanungo, J. Therm. Anal. 20 (1981) 459.
[43] S. Mathew, C.G.R. Nair, K.N. Ninan, Bull. Chem. Soc. Jpn. 64 (1991) 3207.
[44] S.H. Rahaman, H.-K. Fun, B.K. Ghosh, Polyhedron 24 (2005) 3091.
[45] Z. Han, Y. Gao, X. Zhai, H. Song, Inorg. Chem. Commun. 10 (2007) 1079.
[46] H. Chowdhury, S.H. Rahaman, R. Ghosh, S.K. Sarkar, M. Corbella, B.K. Ghosh, Inorg. Chem. Commun. 9 (2006) 1276.
[47] X.-L. Chen, Y.-J. Yao, H.-M. Hu, S.-H. Chen, F. Fu, Z.-X. Han, T. Qin, M.-L. Yang, G.-L. Xue, Inorg. Chim. Acta 362 (2009) 2686.
[48] C. Maxim, T.D. Pasatoiu, V.C. Kravtsov, S. Shova, C.A. Muryn, R.E.P. Winpenny, F. Tuna, M. Andruh, Inorg. Chim. Acta 361 (2008) 3903.
[49] A. Majumder, G.M. Rosair, A. Mallick, N. Chattopadhyay, S. Mitra, Polyhedron 25 (2006) 1753.
[50] S. Basak, S. Sen, S. Banerjee, S. Mitra, G. Rosair, M.T.G. Rodriguez, Polyhedron 26 (2007) 5104.
[51] D. Das, B.G. Chand, K.K. Sarker, J. Dinda, C. Sinha, Polyhedron 25 (2006) 2333.
[52] J.C. Bonner, M.E. Fisher, Phys. Rev. A135 (1964) 640.
[53] Y.-Y. Liu, J.-F. Ma, J. Yang, J.-C. Ma, Z.-M. Su, Cryst. Eng. Commun. 10 (2008) 894.
[54] (a) S. Su, Z. Guo, G. Li, R. Deng, S. Song, C. Qin, C. Pan, H. Guo, F. Cao, S. Wang, H. Zhang, Dalton Trans. 39 (2010) 9123;
(b) L.-J. Zhang, J.-Q. Xu, Z. Shi, X.-L. Zhao, T.-G. Wang, J. Solid State Chem. 173 (2003) 32;
(c) A.M. Atria, G. Corsini, L. González, M.T. Garland, R. Baggio, Acta Crystallogr., Sect. C 65 (2009) m241.
[55] (a) J. Bickley, R.P. Bonar-Law, M.A. Borrero Martinez, A. Steiner, Inorg. Chim. Acta 357 (2004) 891;
(b) S. Zhanga, Y. Caoa, H. Zhanga, X. Chaia, Y. Chen, J. Solid State Chem. 181 (2008) 399.
[56] D.A. McMorran, P.J. Steel, J. Chem. Soc., Dalton Trans. (2002) 3321.
[57] L.K. Thompson, F.L. Lee, E.J. Gabelb, Inorg. Chem. 27 (1988) 39.
[58] L. Carlucci, G. Ciani, D.M. Proserpio, S. Rizzato, Cryst. Eng. Commun. 4 (2002) 121.
[59] C.C. Addison, N. Logan, S.C. Wallwork, C.D. Garner, Q. Rev. Chem. Soc. 25 (1971) 289.
[60] T. Otieno, S.J. Rettig, R.C. Thompson, J. Trotter, Inorg. Chem. 34 (1995) 1718.
[61] G. Psomas, C.P. Raptopoulou, L. Iordanidis, C. Dendrinou-Samara, V. Tangoulis, D.P. Kessissoglou, Inorg. Chem. 39 (2000) 3042.